Hydrodynamic and solid residence time distribution in a Circulating Fluidized Bed : experimental and 3D computational study

Régis ANDREUX[1], Geoffrey PETIT[1-2-3], Mehrdji HEMATI[2], Olivier SIMONIN[3]

1: Institut Français du Pétrole (IFP), Solaize, France

Chemical Engineering Dpt.

Institut Français du Pétrole

Solaize B.P.3, 69390 Vernaison , France

regis.andreux@ifp.fr

2: Laboratoire de Génie Chimique (LGC), Toulouse, France

3: Institut de Mécanique des Fluides de Toulouse (IMFT), France

Abstract – Vertical profiles of local pressure, horizontal profiles of net vertical solid mass flux, and residence time distributions (RTD) of the solid phase are experimentally assessed in the riser of a small scale cold Circulating Fluidized Bed of 9 m high having a square cross section of 11×11 cm. Air (density 1.2 kg/m^3, dynamic viscosity 1.8×10^{-5} Pa.s) and typical FCC particles (density 1400 kg/m^3, mean diameter 70 mm) are used. The superficial gas velocity is kept constant at 7 m/s while the solid mass flux ranges from 46 to 133 kg/m^2/s. The axial dispersion of the solid phase is found to decrease when increasing the solid mass flux. Simultaneously, 3D transient CFD simulations are performed to conclude on the usability of the eulerian-eulerian approach for the prediction of the solid phase mixing in the riser. The numerical investigation of the solid mixing is deferred until later since the near-wall region where the solid phase downflow and mixing are predominant is not well predicted in spite of well-predicted vertical profiles of pressure.

1. Introduction

Solid phase residence time distribution in the riser reacting zone is a major issue in the Fluid Catalytic Cracking process which converts large quantities of heavy liquid oils to lighter and more valuable gas products in refineries. Indeed, the smaller the residence time distribution of the solid phase is (when combined with gas plug flow and high gas-particle transfer), the higher the selectivity of the cracking catalytic reaction is, leading to low coke and undesirable gas production.

1

During the last ten years, the Institut Français du Pétrole has intensively studied the hydrodynamics of the reacting riser zone with its academic partners in order to optimize its Fluid Catalytic Cracking process (Figure 1 : *The R2R resid Fluid Catalytic Cracking process (Axens-IFP-Stone & Webster Inc.- TOTAL technology).*

, using both experimental and CFD approaches ([1-6]). In the context of this Research and Development program, an experimental database related to the solid phase residence time distribution in an hydrodynamic regime similar to the industrial one is required to understand and model the phenomena. Then, vertical profiles of local pressure, horizontal profiles of net vertical solid mass flux, and residence time distributions (RTD) of the solid phase are experimentally assessed in the riser of a small scale cold Circulating Fluidized Bed of 9 m high having a square cross section of 11×11 cm. Air (density 1.2 kg/m^3, dynamic viscosity 1.8×10^{-5} Pa.s) and typical FCC particles (density 1400 kg/m^3, mean diameter 70 mm) are used.

The objectives of this work are then :

- to establish a database which includes both local hydrodynamics (local pressure drop and local vertical solid mass flux) and solid residence time distribution descriptions.

- to relate the solid residence time distribution to the solid mixing in the frame of a rough approach with a global 1D-equation([7-10]) :

$$u\frac{\partial C}{\partial z} + \frac{\partial C}{\partial t} = D_{ax}\frac{\partial^2 C}{\partial z^2} \qquad (1)$$

 where U is the superficial solid phase velocity in the riser, C is the local concentration of a tracer carried by the particles at the vertical position z, , and D_{ax} is the vertical dispersion coefficient of the tracer.

- to test the usability of the eulerian-eulerian CFD approach for the prediction of the solid phase mixing in the riser.

2. Experimental set-up

The cold pilot-scale CFB is presented in Figure 2. The riser consists of four elements, two meters long, and one element, one meter long, all with a square cross-section of 11×11 cm. In order to visualise the gas-solid flow, all is made of transparent altuglass. Humidified air (1.2 kg/m^3, $1.8 \ 10^{-5}$ Pa.s) is injected at the bottom of the riser through a perforated plate containing sixty-four 8 mm-diameter holes. Previous experimental studies had shown that electrostatic phenomena disappear for a relative humidity greater than 80% ([1]). The gas flow rate is measured using a rotameter before injection in the riser. FCC powder (1400 kg/m^3, 70 μm) is injected horizontally by a 100 mm-diameter L-valve designed-based on [11-12], and modified to obtain a very stable solid injection with no solid accumulation when operating the CFB : the L-valve is now supplemented with a slide valve, another aeration tap, and is ended by a diaphragm with a square cross-section of 25*25 mm through which the injected gas-particle suspension has a constant horizontal velocity fixed at 2.5 m/s. The horizontal injection is made at 100 mm above the distributor. Both phases are conveyed vertically upward and are separated at the top of the riser with two classic Swift-cyclones. Then particles move downwards into a first dense fluidized bed for storage or are diverted into a previously empty fluidized tank for global solid mass flux measurement. Gas escapes from the cyclone through ducts equipped with Pitot tubes, confirming gas flow rate measurements. Experiments were carried out at a superficial velocity of 7 m/s and solid circulation mass fluxes from 46 to 133 kg/m2s, equivalent to solid/gas mass loading ratios of 5.5 to 15.8.

3. Experimental techniques

3.1. Hydrodynamics characterization

Pressure probes spread along the riser provide axial pressure profiles with an acquisition frequency of 20 Hz during a time period of 5 minutes. The distance between two consecutive

pressure taps is : 100 mm along the first meter, 200 mm along the second meter, and 500 mm along the rest of the riser.

An iso-kinetic sampling probe designed based on [10;13] provides the time-averaged local upwards and downwards solid mass flux. Horizontal profiles are established at 8.50 m above the bottom distributor, and the horizontal distance between two sampling points is 5 mm.

3.2. RTD measurements and analysis

Solid tracing NaCl crystals injected in the connecting point between the L-valve and the riser and sampled at the top of the riser provide the Residence Time Distribution of the solid phase. The tracer is assumed to be homogeneously distributed at the sampling point elevation since the restricting top riser section induces a high local solid mixing which is visually observed. The NaCl crystals have been crushed and sieved (diameter=55-60 µm) to obtain a final free fall velocity equal to the one of the transported particles. NaCl crystals are protected against humidity during the mock-up operation being stored at 100°C and cooled before the impulse injection thanks to a holder pressurised at 3 bars (Figure 3). Each measurement requires the injection of 50 grams of NaCl. The particles are continuously sampled at the centre top of the riser during a time period of 20 to 30 times the geometrical residence time of the solid phase. The particles are continuously sampled using a 10 mm ID probe (Figure 4), separated from the sampled gas in a cyclone and then collected in the 15 mm cyclone dipleg. 15 initially open valves are spread along the cyclone dipleg and are closed successively when sampling. The resulting 15 samples are then treated to obtain the amount of sampled tracer along the time as follows:

- The sampled powder containing FCC particles and NaCl crystals is put in distilled water at fixed temperature. The NaCl is then dissolute.

- The FCC particles are removed from the solution by filtration.

- The electrical conductivity of the filtered solution is measured and converted into a salt concentration using a calibrating curve previously determined (the presence of the FCC particles has been verified not to modify the conductivity measurement).

Each measurement is repeated three times at different days. The presented results are the average values of the three measurements.

Only a fraction of the total solid flux is sampled at the riser outlet. Thus, only a part of the injected salt is recovered. Using the previously mentioned assumption of homogenously distributed tracer on the sampling cross section, the total mass of tracer, m_{salt}^{capt}, traveling through the riser section during the sampling period is given by:

$$m_{salt}^{capt} = \sum_{i=0}^{n} C_i \, G_s \, S_R \, \Delta t_i \qquad (2)$$

where Ci is the tracer mass concentration in the sample i, with $i=[1-15]$, Δt_i, the sampling period of the sample i, G_s the average solid mass flux on the sampling cross section, S_R, n the number of samples during the sampling period.

The accuracy rate of the tracer recovery, δ, is defined as follows :

$$\delta = \left(\frac{m_{salt}^{capt}}{m_{salt}^{inj}} - 1 \right) x \, 100 \qquad (3)$$

where m_{salt}^{inj} is the mass of the injected tracer. Then, a perfect sampling corresponds to $\delta = 0$. An intrinsic error of 5 % on the sampling method is acceptable. Since the solid mass flux measurement technique error is of 5 %, the considered acceptable value for δ is consequently 10 %. Note that a low δ value will confirm the previously mentioned assumption of homogenously distributed tracer on the sampling cross section.

The Residence Time Distribution of the solid phase, $E(t_i)$, is related to the tracer concentration, C_i, in each sample i along the sampling period :

$$E(t_i) = \frac{C_i}{\sum\limits_{i=0}^{\infty} C_i \Delta t_i} \tag{4}$$

The average residence time of the solid phase, $\bar{t}$, is defined as:

$$\bar{t} = \int_0^{\infty} t E(t) dt \approx \sum_{i=0}^{\infty} t_i E(t_i) \Delta t_i \tag{5}$$

The median residence time, $\overline{t_{0.5}}$, is introduced. It is defined as the required time to recover 50 % of the injected tracer and is calculated as follows:

$$\frac{1}{2} m_{salt}^{inj} = \int_0^{\overline{t_{0.5}}} E(t) dt \tag{6}$$

Practically, $\overline{t_{0.5}}$ is visually determined on the cumulative residence time distribution curve since the rigorous calculation should require a more accurate RTD discretization than the one provided by our experimental technique.

In a similar way, $t_{0.1}$ and $t_{0.9}$ are introduced and defined as the required time to recover 10 % and 90 % of the injected tracer, respectively. The spread of the residence time distribution, S, is then defined as :

$$S = \frac{t_{0.9} - t_{0.1}}{t_{0.5}} \tag{7}$$

4. Modeling of the gas-solid two-phase flow

4.1. Principle

The model has been previously tested and validated in the dense and circulating regimes with Geldart-A, B, and D particles ([14-23]). It is referenced as the k-ε/q$_2$^{2}-q$_{12}$ two-fluid model. Governing equations for the fluid phase can be derived directly from the local instantaneous conservation equations in single-phase flow, by density-weighted averaging with, in addition, average balances of mass, momentum and energy at the surfaces of the inclusions.

Within the framework of the kinetic theory on diluted gases, one can obtain a general transport equation for any property of the dispersed phase derived from Boltzmann's equation ([24]). Supplemented by the theory of granular medium with inelastic spheres ([25]) and inter-phase coupling in mean and turbulent fields ([26]), one can obtain a set of particulate phase governing equations.

Then, similar mass (Eq. 1) and momentum (Eq. 2) transport equations are obtained for both phases:

$$\frac{\partial \alpha_k \rho_k}{\partial t} + \frac{\partial \alpha_k \rho_k U_{k,i}}{\partial x_i} = 0 \tag{8}$$

$$\alpha_k \rho_k \left(\frac{\partial U_{k,i}}{\partial t} + U_{k,j} \frac{\partial U_{k,i}}{\partial x_j} \right) = -\frac{\partial \tau_{k,ij}}{\partial x_j} - \alpha_k \frac{\partial P_1}{\partial x_i} + \mathrm{I}_{k,i} + \alpha_k \rho_k g_i \tag{9}$$

where subscript k refers to fluid phase (k=1) or solid phase (k=2). $\tau_{2,ij}$ is the stress for phase k, expressed as $\tau_{k,ij} = \alpha_k \rho_k R_{k,ij} + \Theta_{k,ij}$. $R_{k,ij}$ and $\Theta_{k,ij}$ are, respectively, turbulent and viscous stresses for the fluid phase, or kinetic and collision stresses for the solid phase. $\mathrm{I}_{k,i}$ corresponds to the mean momentum inter-phase exchange after subtracting the mean gas pressure contribution.

$\mathrm{I}_{k,i}$ is obtained by averaging of the drag force exerted by the fluid on any discrete particle and written in terms of the local instantaneous turbulent relative velocity $v_{r,i}$ between the two

phases, so that, $I_{1,i} = -I_{2,i} = \alpha_2 \rho_2 \frac{1}{\tau_{12}^F} V_{r,i}$, where $\tau_{12}^F = \left(\frac{3}{4} \frac{\rho_1}{\rho_2} \frac{C_d}{d_p} \langle\!\langle |v_r| \rangle\!\rangle_2 \right)^{-1}$ is the mean particle

relaxation time. The drag coefficient C_d^s for a single isolated spherical particle is modified to account for the effect of surrounding particles ([27-28]).

$V_{r,i} = < v_{r,i} >_2 = U_{2,i} - U_{1,i} - V_{d,i}$ is the average of the local relative velocity between the two phases, written in terms of the separate mean phase velocities, $U_{k,i}$, and the fluid-particle

turbulent drift velocity, $V_{d,i}$, which represents the turbulent correlation between the instantaneous particle distribution and the turbulent fluid velocity field ([29]). $V_{d,i}$ is accounting for the transport of the dispersed phase by the large scale fluid turbulent motion and is modeled, in first approximation, using the following gradient approximation,

$$V_{d,i} = -D_{12}^t \left[\frac{1}{\alpha_2} \frac{\partial \alpha_2}{\partial x_i} - \frac{1}{\alpha_1} \frac{\partial \alpha_1}{\partial x_i} \right]$$ (10)

with the dispersion coefficient D_{12}^t proportional to the fluid-particle velocity covariance $q_{12} = <u''_{1,i} u''_{2,i}>_2$ and an eddy-particle interaction time τ_{12}^t, characterizing the fluid turbulence experienced ("viewed") by the particles. This fluid-particle turbulent drift velocity allows to ensure the consistency of the model for the limit case of very small particles which behaves as tracers in the gas and becomes negligible for very coarse particles when the mean particle relaxation time is much larger than the fluid turbulence time macroscale.

The stress tensor of the gas phase is modeled in the framework of the k-ε model with inter-phase coupling terms in the turbulent kinetic energy and viscous dissipation transport equations ([30-31]). The eddy – viscosity expression is modified to account for the presence of particles ([32]).

The stress of the particulate phase is modeled with kinetic and collision viscosity given by the Boussinesq approximation. They are determined as a function of the granular temperature, obtained solving the fluctuating energy equation of the solid phase.

The inter-phases coupling on a small scale is taken from [33] with a transport equation for the covariance between the velocity fluctuations of the two phases. Closure modeling of the fluid – particle covariance stresses is eddy-viscosity based.

One should refer to the different cited papers if details are required.

4.2. Unsteady three-dimensional numerical conditions

The simulations are completed using *Saturne_Polyphasique@Tlse*, a multi-phase flow numerical code property of "Electricité de France" (EDF) and developed with its academic partners the IMFT and LGC for the dense and circulating fluidized beds applications, with the two-fluid modeling approach described in the previous part. All the simulations are realized with a 3-D mesh (31000 cells).

The used mesh represents in a faithful way the real riser. It is represented by 10 cells for the width (Ox) of 11 cm (cells are smaller near the walls than in the centre of the riser), 312 cells for the height (Oy) of 9 m and 10 cells for the depth (Oz) of 11 cm. The reactor was simulated during about 50 s and the presented results are time averaged on last 20 physical seconds corresponding to predictions in established regime. We consider the permanent regime achieved when the predicted total mass of catalyst in the riser becomes nearly time independent. For our calculations, it is obtained after about ten physical seconds.

More over, one physical second is simulated in 40 hours CPU on Silicon Graphics computer. The time step is of 2.10^{-4} s. The initial conditions used are a volumetric air flow of 305 m^3/h, i.e. a velocity of 7 m/s, and a solid mass flux of 133 kg/m²/s. The calculation is initialized without solid in the riser. The boundary conditions used are elastic bouncing for the particles and turbulent wall-function for the gas.

5. Results

5.1. Hydrodynamic characterization of the riser

5.1.1. Vertical characterization

The total riser pressure drop is multiplied by 6 when the solid mass flux increases from 46 up to 133 kg/m²/s (Figure 6).The numerical prediction of the total pressure drop is in good agreement with the experimental data, and the CFD code then gives good predictions of the solid retention in the riser.

Based on the vertical pressure gradients profiles (Figure 7a), the riser is always divided into two regions :

- The acceleration zone, characterized by a strong variation of the pressure gradient, which height increases with the solid mass flux. This behavior is well-accepted and has been extensively studied in the literature.

- The established zone, characterized by a pressure gradient almost independent from the height.

The simulation (solid mass flux of 133 kg/m^2/s) describes well the short entry zone, having a high mean pressure drop as a result of the solid feeding (Figure 7b). The decreasing pressure drop along the riser is in good agreement with the experimental data.

5.1.2. Radial characterization

Based on the horizontal profiles of the vertical net solid mass flux (Figure 8a), the riser is divided into two regions :

- The core region where the solid mass flux is nearly constant at lower solid mass fluxes. At higher solid mass flux, the horizontal profile is parabolic in shape.

- The near-wall region where the local solid mass flux greatly decreases.

Intermittent solid downwards flow at the wall is visually observed but is never detected by our 4 mm ID probe (even when placed at 5 mm from the wall). The thickness estimation of the down flow region is then lower than 3 mm.

The shape of the predicted solid mass flux profile in the core region is somewhat flat (Figure 8b). The near-wall region is not well-predicted as no solid down flow is predicted. Consequently, the center value is far higher than the measured one. Then, one can intuitively conclude that residence time distribution CFD predictions will tend toward plug flow.

The most relevant explanation for the numerical prediction discrepancies is the insufficient discretization of the solid down flow near-wall region which should be described by at least

10

three or four cells mesh. However, the resulting size mesh will be of the order of 500 μm which leads to very small time step and then prohibitive CPU time computation. Then, the numerical investigation of the solid mixing is deferred until later since the near-wall region where the solid phase downflow and mixing are predominant is not well predicted in spite of well-predicted vertical profiles of pressure.

5.2. Mixing characterization of the riser

5.2.1. Measurement validation

Tracer recovery is very accurate since the maximum of the accuracy rate, δ, is of the order of 10 % (Table 2). The experiments are well-reproducible (Figure 9). The previously mentioned assumption of homogenously distributed tracer on the sampling cross section is confirms by the RTD measurements obtained in two different points of the sampling riser section (Figure 10).

5.2.2. Results and discussion

Tightness of the RTD curves decreases when increasing the solid mass flux (Figure 11a-e), particularly at low solid mass flux, as shown by the spread coefficient, S (Figure 12b) : S decreases from 3 to 2 when the solid flux increased from 46 to 76 kg/m²/s and is nearly constant beyond. The averaged and the median residence times, $\bar{t}$ and $t_{0.5}$ respectively, decreases from 14 s to 6 s and from 8.6 s to 5.5 s when increasing the solid mass flux from 46 kg/m^2/s to 133 kg/m^2/s (Figure 12a).

The consequent non intuitive conclusion of these trends is that an increase in the solid mass flux at constant gas velocity makes the solid phase tend toward plug flow in the studied fluidizing regime. Such peculiar trend has already been observed by Rhodes [1] with Geldart-A particles.

However, it has been commonly believed that the solids backmixing in CFB risers are mainly associated with :

- the solids downflow in the annulus region.

- the dense bottom zone treated as a perfectly mixed dense bed.

Then, solids residence time distribution and mean value should increase with increasing solids flux since the downflowing annulus region and the dense bottom zone height increase with the increase of solids circulation rate. Consequently, some other mechanism should be introduced to explain the observed trends, probably related to the cohesion effects since it has never been reported with Geldart-B particles. Some other experimental techniques should be used to do so. In such a way, a further paper will present an intensive experimental study of the CFB, based on pressure drop frequency analysis and local solid mass flux assessments at different riser elevations, completed with both gas and solid phases RTD measurements.

6. Modelling the solid phase RTD

In a first approach, the solid phase residence time distribution is related to the solid mixing in the frame of the classic chemical engineering approach with a global 1D-equation assuming perfect horizontal mixing (*i.e.* Plug flow with Axial Dispersion, PAD) :

$$u\frac{\partial C}{\partial z} + \frac{\partial C}{\partial t} = D_{ax}\frac{\partial^2 C}{\partial z^2} \tag{11}$$

where U is the superficial solid phase velocity in the riser, C is the local concentration of a tracer carried by the particles at the vertical position z, , and D_{ax} is the global vertical dispersion coefficient of the tracer.

The global Peclet number, Pe, is introduced and defined as :

$$Pe = \frac{UL_r}{D_{ax}} \tag{12}$$

where L_r is the total vertical distance between the tracer injection and sample points.

The experimental solid phase RTD is well-reproduced by the PAD model (Figure 13) when the solid mass flux is higher than 60 kg/m²/s confirming the assumption of perfect horizontal mixing. At the opposite, the horizontal mixing is not perfect for the lower solid mass flux of 46 kg/m²/s since the PAD model is not accurate at this operating condition, and a horizontal dispersion coefficient should then be counted in the modeling. Consequently, the effects of the horizontal bottom injection on the whole riser hydrodynamics is higher at low solid mass fluxes. It raises certain questions to our RDT analysis and confirms that more experimental techniques are required.

The resulting calculated global vertical Peclet number, Pe, increases from 14.6 to 20.0 when the solid mass flux is increased from 46 kg/m²/s to 133 kg/m²/s (Figure 14, Table 3).

6. Conclusion

Vertical profiles of local pressure, horizontal profiles of net vertical solid mass flux, and Residence Times Distributions of the solid phase are experimentally assessed in the riser of a small scale cold Circulating Fluidized Bed of 9 m high having a square cross section of 11×11 cm. Air (density 1.2 kg/m^3, dynamic viscosity 1.8×10^{-5} Pa.s) and typical FCC particles (density 1400 kg/m^3, mean diameter 70 mm) are used. The superficial gas velocity is kept constant at 7 m/s while the solid mass flux ranges from 46 to 133 kg/m^2/s.

The riser total pressure drop, *i.e.* the solid retention, increases when increasing the solid mass flux. The riser is vertically divided into two regions : the acceleration zone, characterized by a strong variation of the pressure gradient, which height increases with the solid mass flux, and the established zone, characterized by a constant vertical pressure gradient. The riser is horizontally divided into two regions : the core region where the local vertical net solid mass flux profile is nearly flat at low solid mass flux and gets parabolic in shape when increasing the solid mass flux, and the annulus region where the local solid mass flux greatly decreases with a negative net solid mass flux region which thickness is of the order of 3 mm.

The axial dispersion of the solid phase decreases when increasing the solid mass flux. Such trends has never been reported with Geldart-B particles while it has once with Geldart-A particles. More experiments involving other experimental techniques are required to explain this surprising trend.

A first rough modeling using a global 1D-equation suggests that the horizontal mixing may be perfect at high solid mass flux while it should be counted for at low solid mass flux.

Simultaneously, 3D transient CFD simulations are performed to conclude on the usability of the eulerian-eulerian approach for the prediction of the solid phase mixing in the riser. The numerical investigation of the solid mixing is deferred until later since the near-wall region where the solid phase downflow and mixing are predominant is not well predicted in spite of well-predicted vertical profiles of pressure. The most relevant explanation for the numerical prediction discrepancies is the insufficient discretization of the solid down flow near-wall region which should be described by at least three or four cells mesh. However, the resulting size mesh will be of the order of 500 μm which leads to very small time step and then prohibitive CPU time computation.

Nomenclature

C_d : drag coefficient, dimensionless

$C(t)$: salt concentration, g/g

D_{ax} : axial dispersion coefficient, m²/s

d : diameter, m

d_p : particle mean diameter, m

$E(t)$: residence time distribution, s^{-1}

Gs : solid mass flux, kg/m²/s

m_{salt}^{capt} : captured mass of salt, g

m_{salt}^{inj} : injected mass of salt, g

m_i : mass of the sample "i", g

Pe : Peclet number based on U(=UL/D_{ax}), dimensionless

Pe_s : solid phase Peclet number based on $V_{s0.5}$ ($V_{s0.5}$L/D_{ax}), dimensionless

q_{12} : covariance of the fluid/particle velocity turbulent fluctuations, m²/s²

$q_2{}^2$: fluctuating kinetic energy of the particles, m²/s²

S : span, dimensionless

S_R : cross section riser, m²

$\bar{t}$ **:** average residence time, s

$t_{0.5}$: median residence time, s

U : superficial gas velocity, m/s

$u_{k,i}$: i-component of instantaneous velocity of phase k, m/s

$U_{k,i}$: i-component of mean velocity of phase k, m/s

$u"_{k,i}$: i-component of velocity fluctuation of phase k, m/s

$V_{d,i}$: fluid-particle turbulent drift velocity, m/s

$V_{r,i}$: mean relative velocity between the two phases, m/s

$V_{s0.5}$: velocity of particle with residence time $t_{0.5}$, m/s

Z : height from distributor, m

ΔP_t : total pressure drop in the riser, Pa

Greek letters

α_k : fraction rate of the phase k, dimensionless

ρ_k : density of phase k, kg/m³

$\Theta_{k,ij}$ **:** collisional stress tensor, dimensionless

θ **:** dimensional time (=t/$t_{0.5}$), s

τ_r : recovery rate, dimensionless

τ_{12}^{F} : characteristic time scale of particle entrainment by the fluid motion or particle relaxation time, s

τ_{12}^{t} : time macroscale of the gas turbulence viewed by the particles or eddy-particle interaction time, s

τ_{2}^{c} : characteristic time scale of particle-particle collisions or interparticle collision time, s

Subscripts

1 : continuous phase (air)

2 : dispersed phase (solid)

eq : equivalent particles

tr : transport

t : final free fall

i, j : spatial coordinates

References

[1] R. Andreux, Experimental and numerical study of a gas-solid separator of a cold FCC moke-up (2001), PhD Thesis, Institut National Polytechnique de Toulouse, France.

[2] R. Andreux, M. Hémati, O. Simonin, G.Ferschneider, .Hydrodynamic Investigation of a CFB: Numerical Study and Experimental Validation. Presented Circulating Fluidized Bed Technology VII, Proc. of the 7th Int. Conference on Circulating Fluidized Beds, Niagara Fall, Canada (2002).

[3] T. Gauthier, J. Bayle, P. Leroy, FCC : Fluidization phenomena and technologies*, Oil & Gas Science and Technology, Revue de l'IFP*, 55(2) (2002), pp.187-207.

[4] R. Andreux, J. Verstraete, T. Gauthier, R. Roux., J.-L. Ross, An efficient FCC riser separation system : from R&D to industrial practice, in IFSA – Industrial Fluidization South

Africa, Johannesburg, 16-17 Nov. 2005, Proceedings, A. Luckos and P. Smit eds., 2005, pp. 225-244, South Africa Institute of Mining and Metallurgy.

[5] G. Petit, M. Hémati, O. Simonin, R. Andreux, Experimental and 3D Computational Study of Multiphase Flow Behaviour in a Riser of a FCC Process. Presented at Circulating Fluidized Bed Technology VIII, Kefa Cen (Ed.), Proc. of the 8th Int. Conf. on Circulating Fluidized Beds, Hangzhou, China (2005).

[6] R. Andreux, G. Ferschneider, M. Hémati, O. Simonin, Experimental study of a fast gas-particle-separator, Chemical Engineering Research and Design, submitted in 2006.

[7] M.J. Rhodes, S. Zhou, T. Hirama and H. Cheng, Effects of operating conditions on longitudinal solids mixing in a circulating fluidized bed riser, AIChE Journal, vol.37, 10 (1991), pp. 1450-1458.

[8] K. Smolders and J. Baeyens, Overall solids movement and solids residence time distribution in a CFB-riser, Chemical Engineering Science, 55 (2000), pp. 4101-4116.

[9] R. Bader, J. Findlay and T.M. Knowlton, Gas/solids flow patterns in a 30.5 cm diameter circulating fluidized bed, In P. Basu & J.F. Large, Circulating fluidized bed technology II, Oxford : Pergamon Press. (1988), pp. 123-137.

[10] S. Diguet, Contribution à l'étude de la déshydratation du carbonate de sodium monohydrate en lit fluidise dense et mise en oeuvre en lit fluidise circulant: étude expérimentale et modélisation, Ph.D. dissertation (1996), INP Toulouse, France.

[11] T.M. Knowlton, Non mechanical solids feed and recycle devices for circulating fluidized beds, CFB technology II, Compiègne, France (1988).

[12] W.C. Yang, T.M. Knowlton, L-valve equations, Powder Techn., 77 (1993), pp.49-54.

[13] M. Rhodes, P. Laussmann, A simple non-isokinetic sampling probe for dense suspension, Powder Techn., 79 (1992), pp.141-151.

[14] G. Balzer, A. Boelle, O. Simonin, Eulerian Gas-Solid Modelling of Dense Fluidized Bed, Fluidization VIII, J.F. Large and C. Laguérie, Eds. (1995).

[15] H. Enwald, E. Peirano, A.E. Almstedt, Eulerian two-phase flow theory applied to fluidization, Int. J. Multiphase Flow, 22 (1996), pp 21-66.

[16] J. Begis, G. Balzer, Bi- and Three- Dimensional Numerical Simulation of a CFB: Application to fluidizing regime diagram establishment. *Internal Report HE-44/97/001/A, Laboratoire National d'Dhydraulique, EDF, Chatou, France* (1997).

[17] G. Balzer, Gas-Solid Flow Modelling Based on the Kinetic Theory of Granular Media: Validation, Applications and Limitations, Powder Techn. 113 (2000), pp. 299-309.

[18] E. Peirano, V. Delloume, B. Leckner, Two- or Three-Dimensional Simulations of Turbulent Gas-Solid Flows applied to Fluidization. Chem. Eng. Sc. 56 (2001), pp.4787-4799.

[19] E. Peirano, V. Delloume, F. Johnsson, B. Leckner, O. Simonin, Numerical Simulation of the Fluid Dynamics of a Freely Bubbling Fluidized Bed : Influence of the Air Supply System. Powder Tech. 122 (2002), pp.69-82.

[20] A. Gobin, H. Neau, O. Simonin, J.R. Llinas, V. Reiling, J.L. Sélo., Fluid Dynamic Numerical Simulation of a Gas Phase Polymerisation Reactor, International Journal for Numerical Methods in Fluids, 43 (2003) pp.1199-1220.

[21] J. Soulas, R. Occelli, O. Simonin, L. Tadrist, V. Reiling, Comparison of Dense Gas-Solid Fluidized Bed Predictions from Hard-Sphere Discrete Particle and Two-Fluid Continuum Modeling Approaches, Proc. 5th Int. Conference on Multiphase Flow, ICMF'2004, Yokohama (Japan), paper n° 353.

[22] C. Saulnier, O. Simonin, D. Vedrine, L. Donnat, Eulerian Multiphase Modeling of Feed Injection and Vaporisation in FCC Riser Reactors, In Circulating Fluidized Bed Technology VIII, Kefa Cen (Ed.), Proc. of the 8th Int. Conf. on Circulating Fluidized Beds, Hangzhou (China), International Academic Publishers/Beijing Word Publishing Corporation, pp 328-335 (2005).

[23] O. Batrak, G. Patino, O. Simonin, I. Flour, T. Leguevel, E. Perez Unlike Particles Size Collision Model in 3D Unsteady Polydispersed Simulation of Circulating Fluidised Bed, In

Circulating Fluidized Bed Technology VIII, Kefa Cen (Ed.), Proc. of the 8th Int. Conf. on Circulating Fluidized Beds, Hangzhou (China), International Academic Publishers/Beijing Word Publishing Corporation, pp 370-378. (2005).

[24] H. Grad, On the Kinetic Theory of Rarefied Gas. Com. On Pure and Applied Mathematics, 2 (4), 331-407 (1949).

[25] J.T. Jenkins, M.W. Richman, Grad's 13-Moment System for a Dense Gas of Inelastic Spheres, Arch. Ration. Mech. Anal., 87, 335 (1985).

[26] O. Simonin, Statistical and continuum modelling of turbulent reactive particulate flows. Part 1., Theoretical and experimental modelling of particulate flows, Lecture Series 2000-06, von Karman Institute for Fluid Dynamics (2000), Rhode St Genése, Belgium.

[27] C.Y. Wen, Y.H. Yu, Mechanics of fluidization, Chemical engineering symposium series, 62 (1965), pp. 100-111.

[28] S. Ergun, Fluid flow through packed bed columns, Chem. Eng. Prog. 48 (1952), p.89.

[29] O. Simonin, E. Deutsch, J.P. Minier, Euleian Predictions of the Fluid/Particle Correlated Motion in Turbulent Dispersed Two-Phase Flows. Applied Scientific Research, 51 (1993), 275-283.

[30] S.E. Elgobashi, T.W. Abou-Arab, A Two-Equation Turbulence Model for Two-Phase Flows. Phys. Fluids, 2b4 (1983), 931-938.

[31] O. Simonin, P.L.Viollet, Modeling of Turbulent Two-Phase Jets Loaded with Discrete Particles. Phase-Interface Phenomena in Multiphase Flows, G.F. Hewitt, F. Mayinger, and J.R. Riznic, ed. Hemisphere Publishing Corp., 259-269 (1990).

[32] G. Balzer, O. Simonin, Three Dimensional Numerical Simulation of Two-Phase Flow in Industrial CFB Boiler. Proc. 14th Int. Conf. on Fluidized Bed Combustion, ASME, Vancouver, 2, 1017-1022 (1997).

[33] O. Simonin, Second-Moment Prediction of Dispersed Phase Turbulence in a Particle-Laden Flow. 8th Int. Symp. On Turbulent Shear Flows (1991).

Tableau 1. Physical properties of the FCC particles

Standard conditions	
Pressure [Pa]	10^5
Temperature [°C]	20
Gas (air)	
Density [kg/m^3]	1,2
Dynamic viscosity [Pa.s]	$1,8.10^{-5}$
Solid (particles of FCC)	
Diameter [µm]	70
Density [kg/m^3]	1400
Final free fall velocity [m/s]	0,18
Transport velocity* [m/s]	1,7

: estimated with the Lee&Kim's relation (1990)

Tableau 2. Solid mass flux influence (Z = 8.50 m, Ug = 7 m/s)

n°	G_s (kg/m²/s)	Radial position of the probe	δ (%)	S $\pm$ 0.5 (-)	$t_{0.5} \pm 0.5$ (s)
1	46	*Center (d= 0.055 m)*	*4.0*	2.9	8.8
1[b]			*-9.4*	3.1	8.3
2	60	*Center (d= 0.055 m)*	*2.0*	2.8	6.0
2[b]			*-9.9*	2.9	6.2
3	76	*Center (d= 0.055 m)*	*-11.0*	2.1	5.5
3[b]			*-6.6*	2.1	5.5
4	76	*Quarter (d= 0.0275 m)*	*-10.5*	2.3	4.4
4[b]			*-2.9*	2.1	4.6
5	100	*Center (d= 0.055 m)*	*-3.3*	2.1	5.4
5[b]			*-2.3*	1.8	5.3
6	133	*Center (d= 0.055 m)*	*4.1*	1.8	5.1
6[b]			*7.2*	1.8	4.7

Tableau 3. Peclet number values for different solid mass fluxes

G_s (kg/m²/s)	**46**	**60**	**76**	**100**	**133**
Pe$_s$	2,2	3,4	4,5	4,9	5,3

| Pe | 14,6 | 16,1 | 19,2 | 20,3 | 20,0 |

Figures
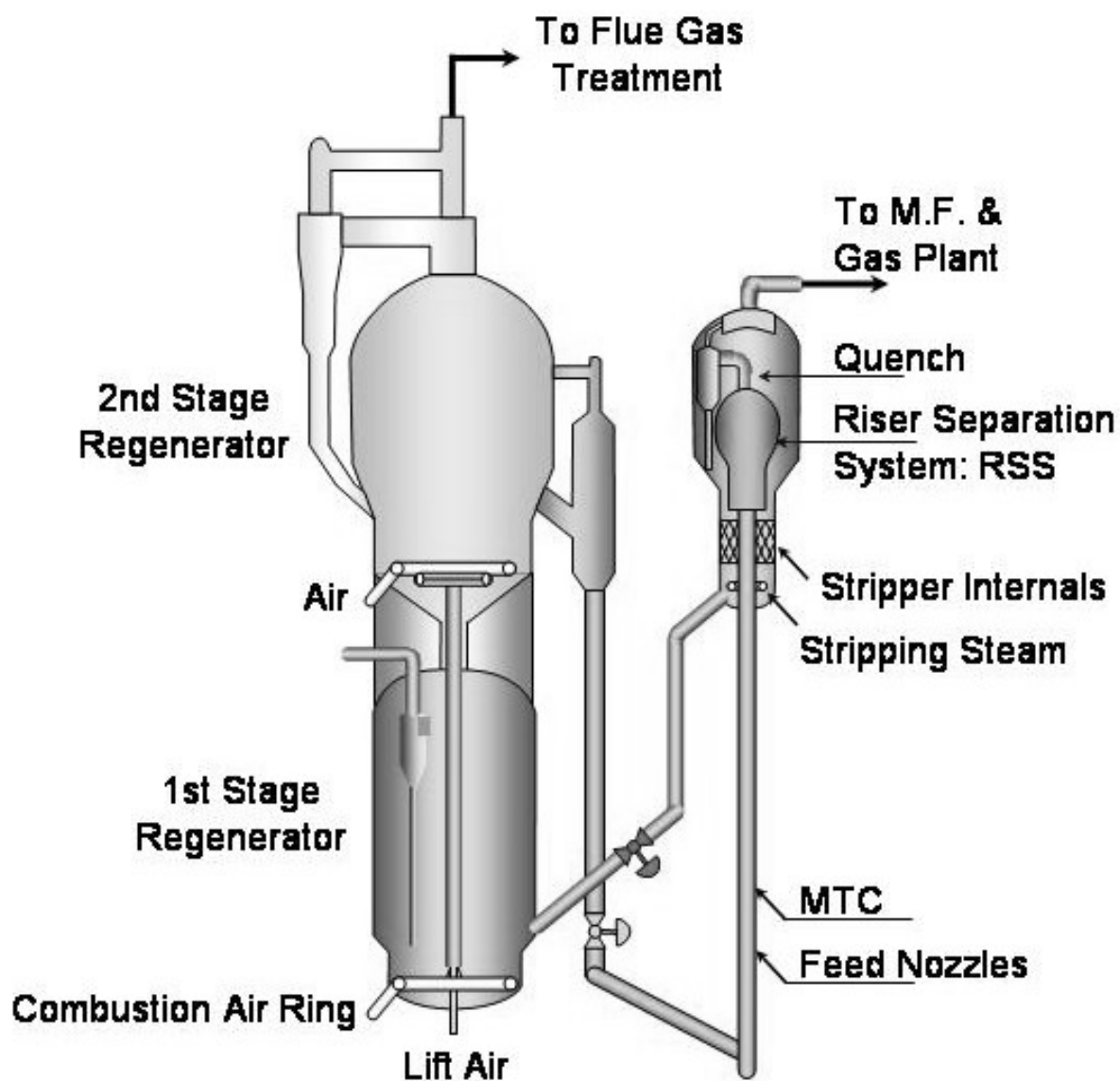
Figure 1 : The R2R resid Fluid Catalytic Cracking process (Axens-IFP-Stone & Webster Inc.-

TOTAL technology).
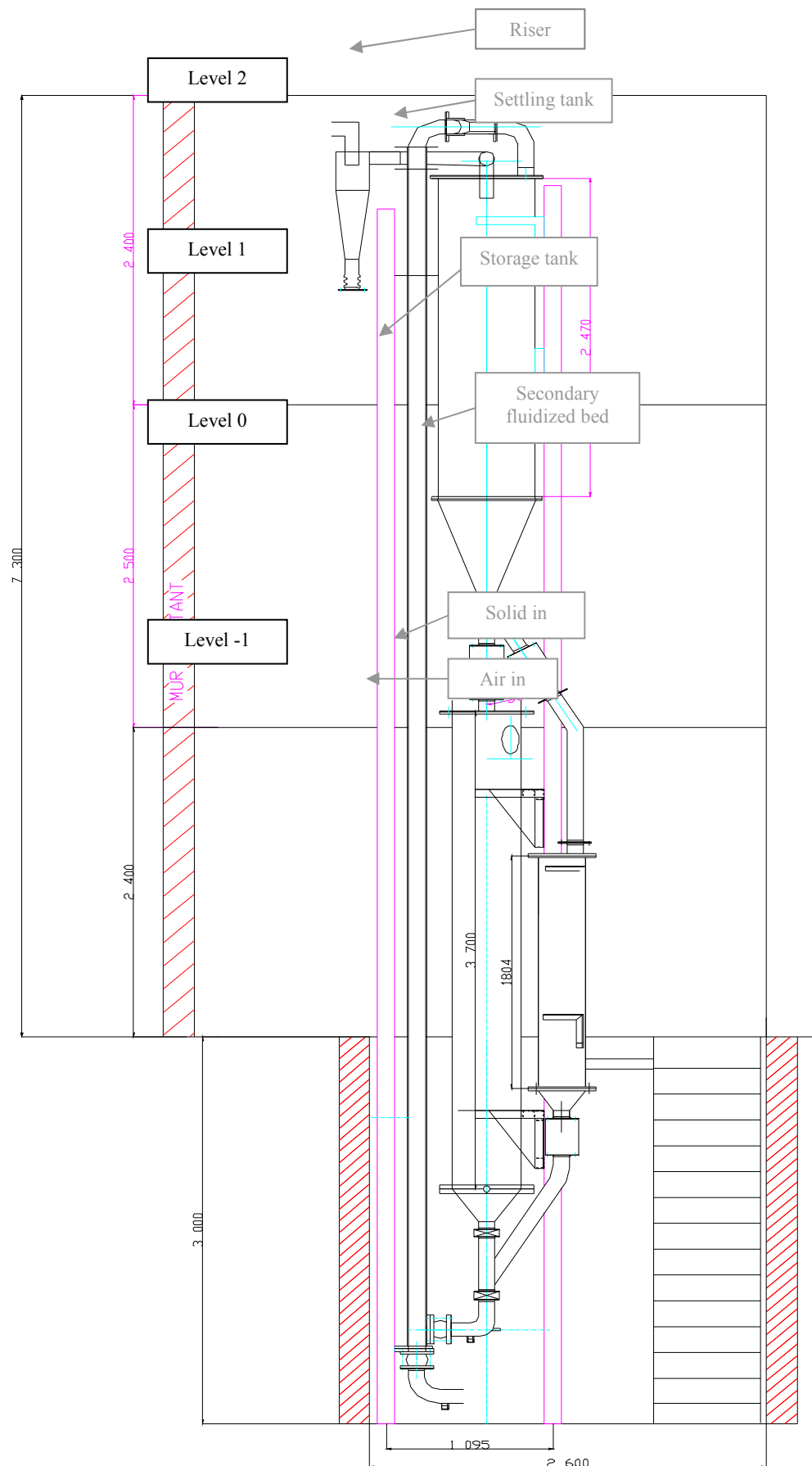
Figure 2 : Schematic diagram of the experimental apparatus
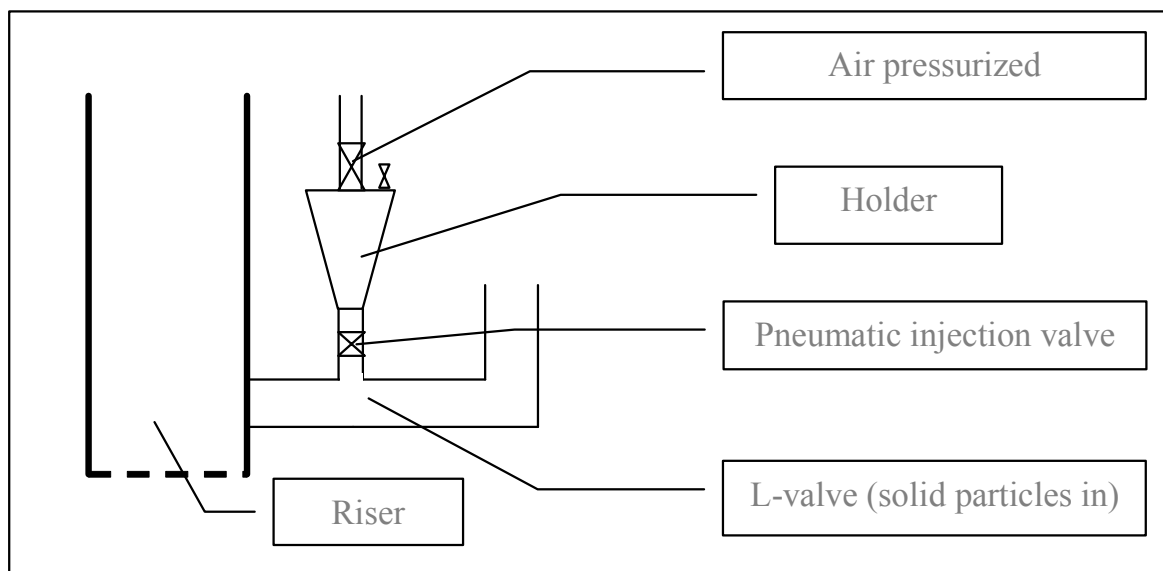
Figure 3 : Injection system for the salt tracer

Valve n°	Spacement
1 à 6	2 cm
7 à 12	5 cm
13 à 15	7 cm
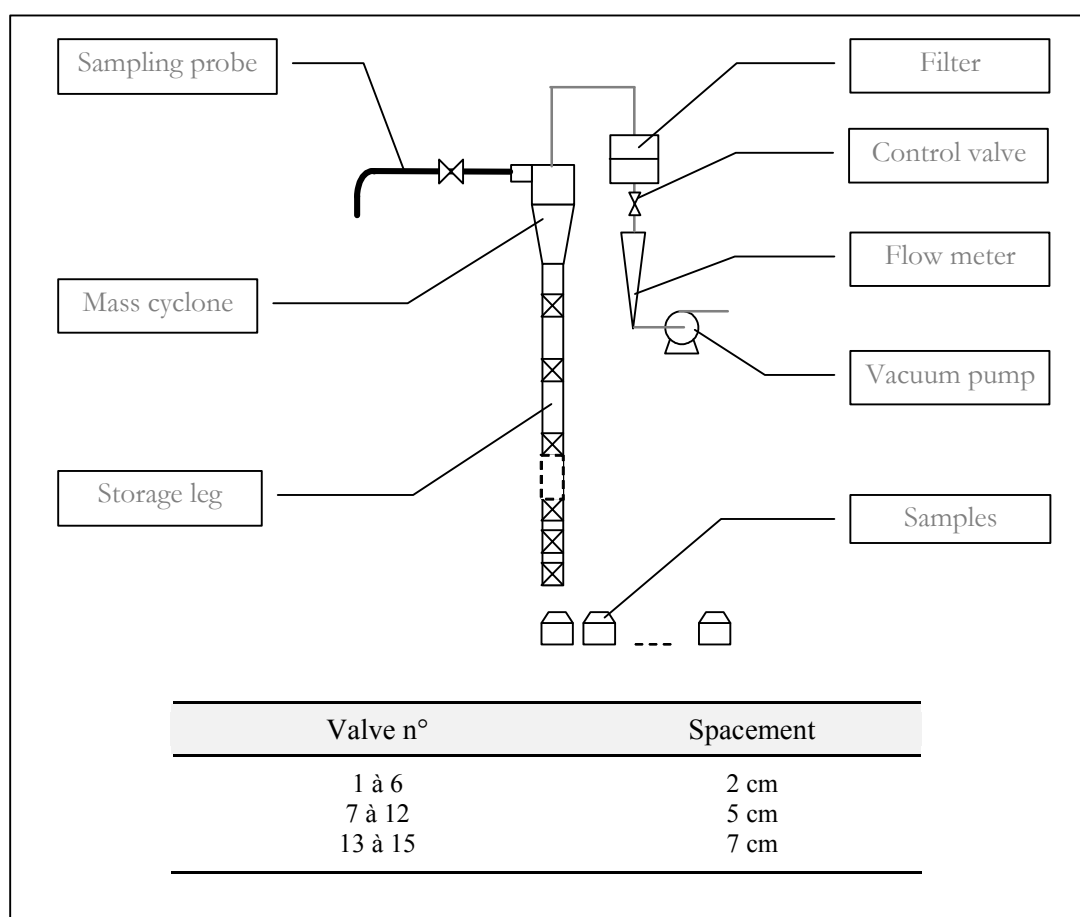
Figure 4 : Sampling system for the determination of the solids RTD.
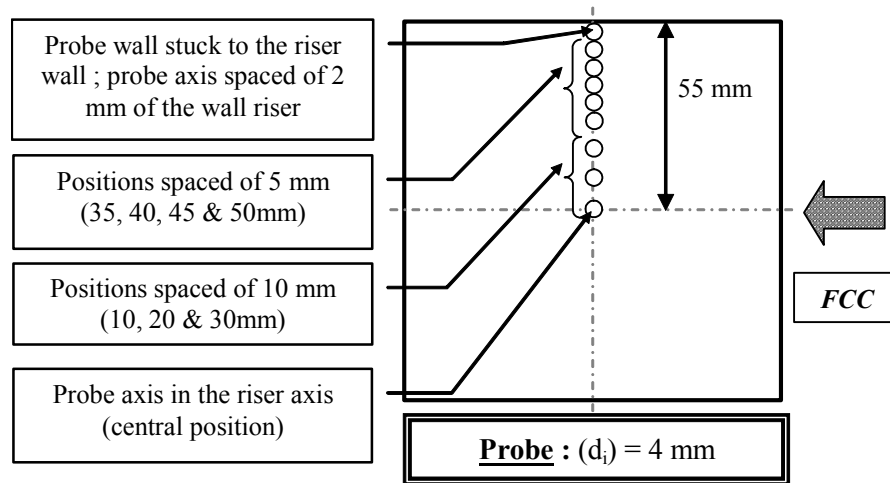
Figure 5 : Various radial positions used for the determination of solid mass fluxes radial

profiles .
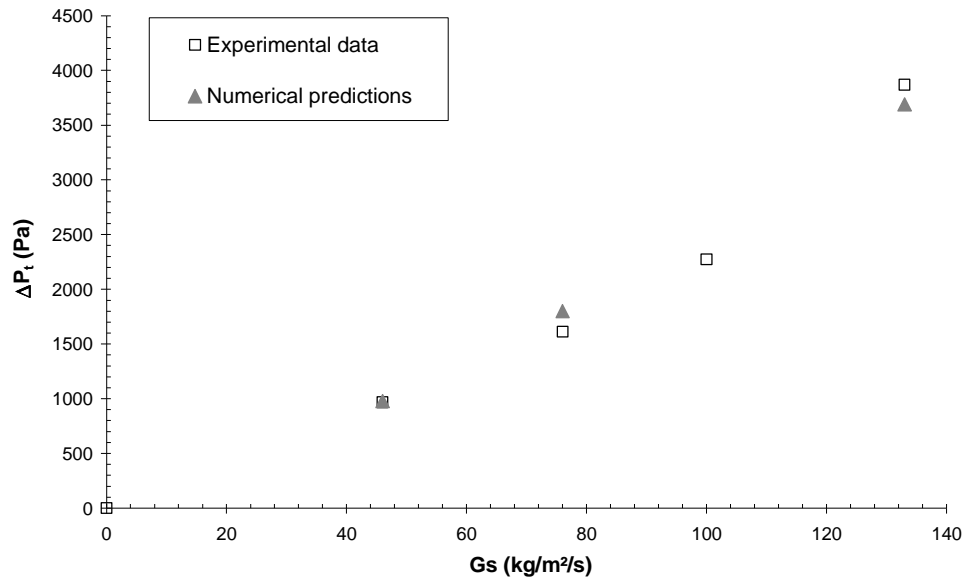
Figure 6 : Evolution of the total pressure drop in the riser with the solid mass flux.
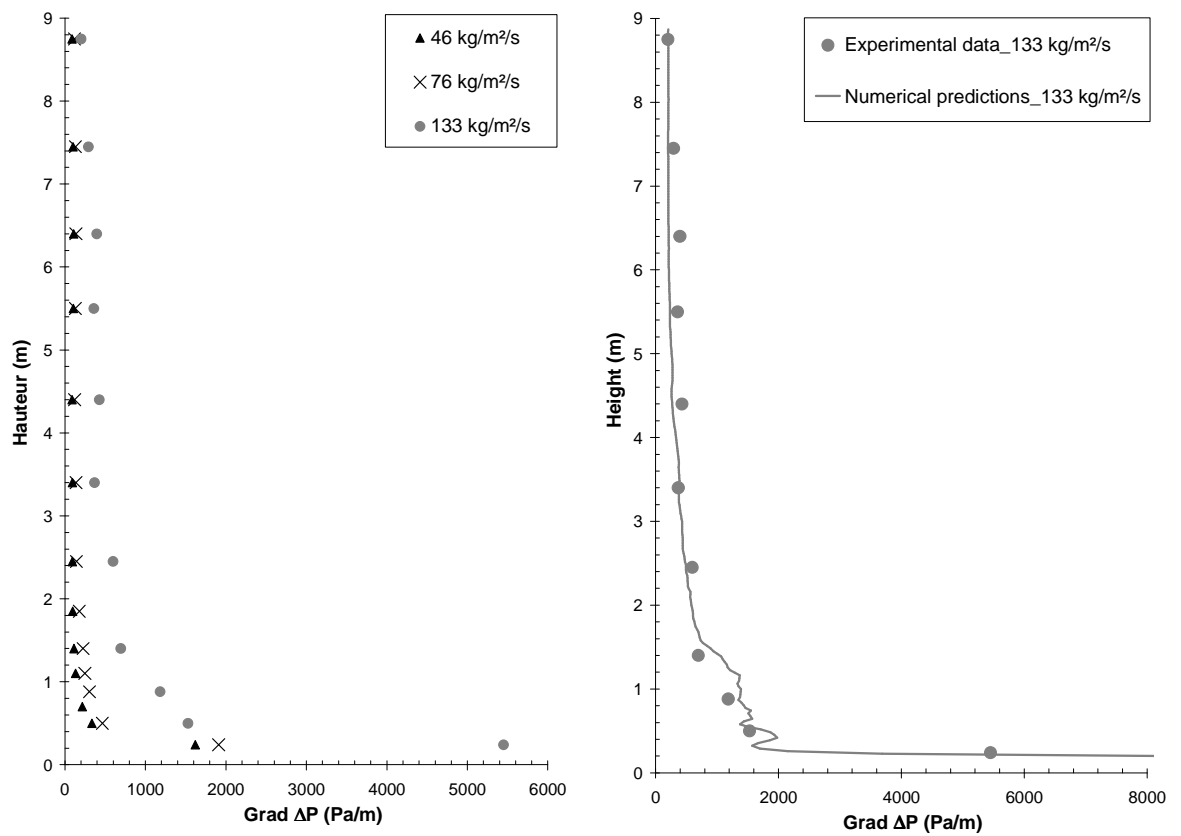
Figure 7 : Vertical pressure gradients profiles. Experiments (a, left) and numerical data (b,right).
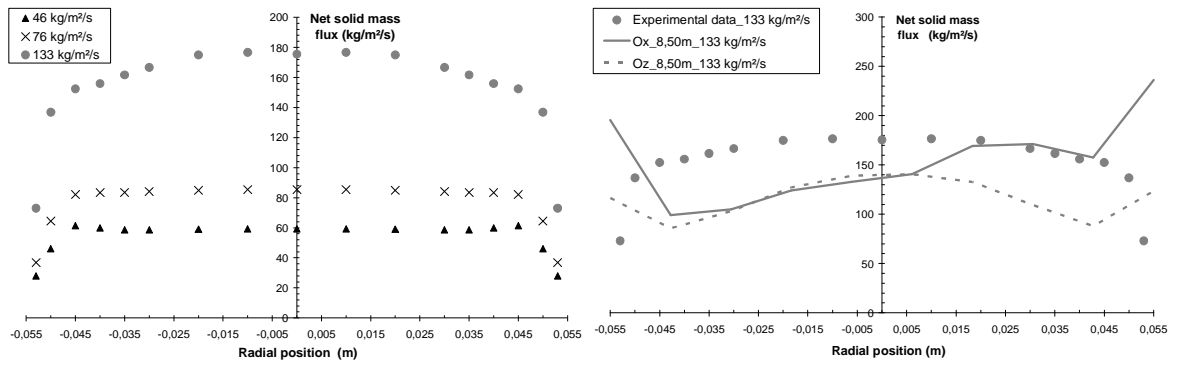
Figure 8 : Horizontal solid mass flux profiles. Experiments (a, left) and numerical data (b,right).
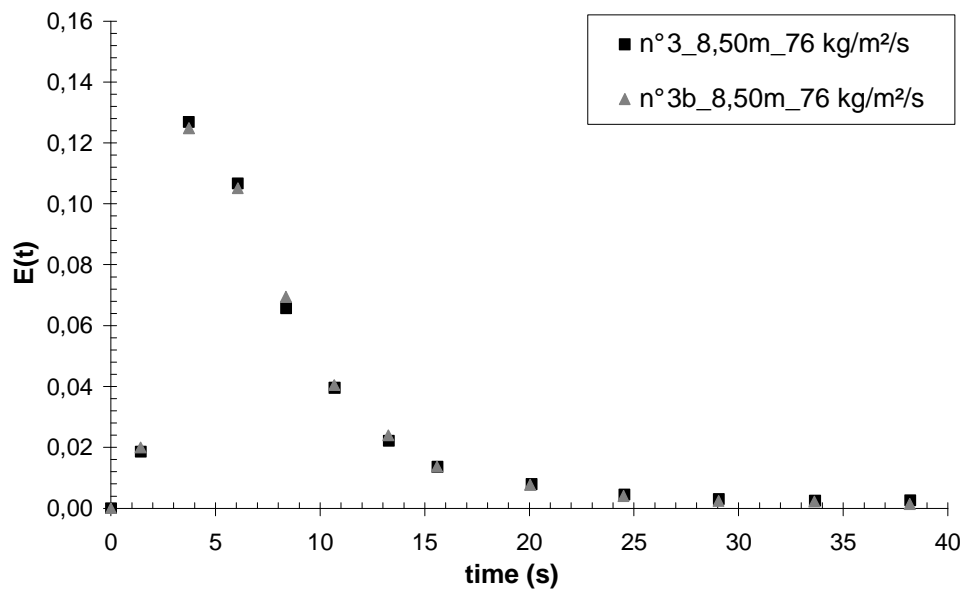
Figure 9 : Reproducibility of the RTD measurement (Gs = 76 kg/m²/s ; Z = 8.50 m).
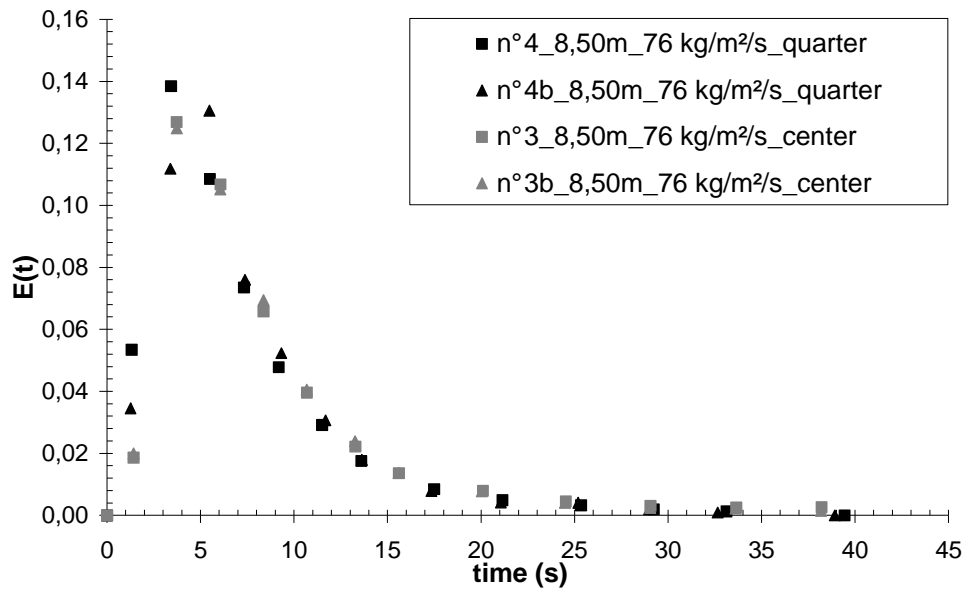
Figure 10 : Confrontation of RTD curves obtained at two radial positions: d= 0.055 m (center)

and d = 0.0275 m (quarter) (Gs = 76 kg/m²/s ; Z = 8.50 m).

(e)
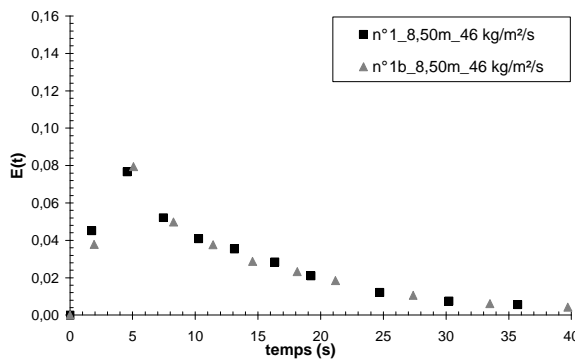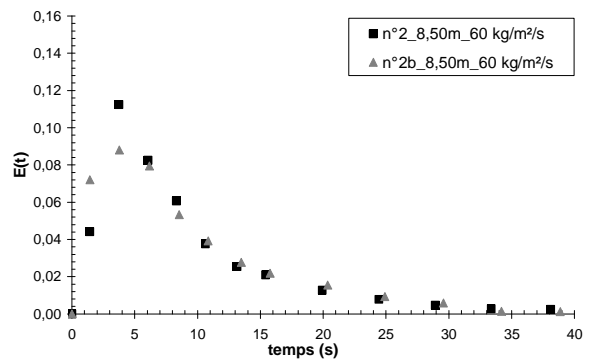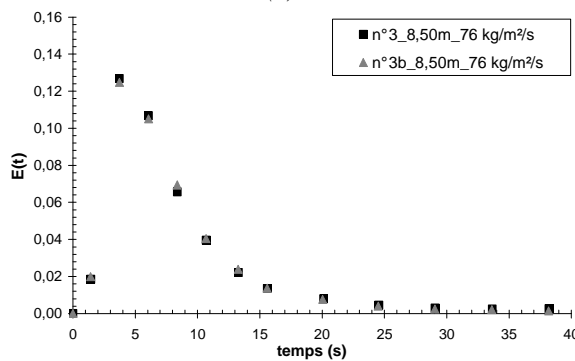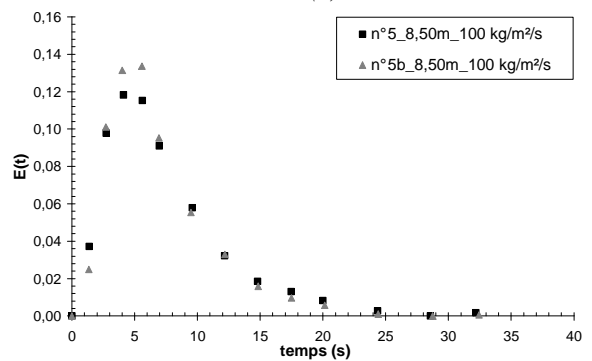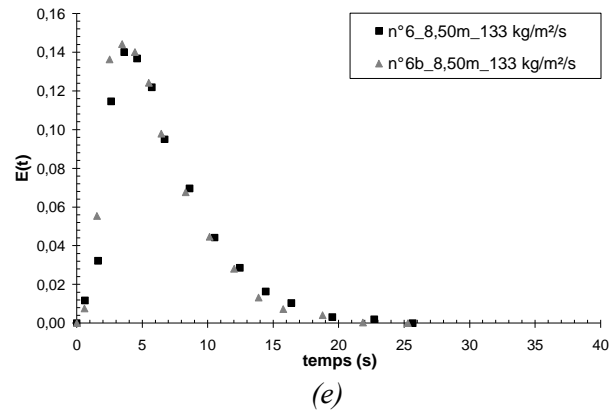
Figure 11 : RTD curves obtained for five solid mass fluxes (in kg/m²/s):
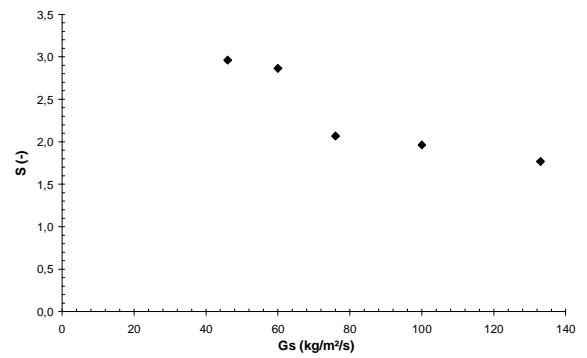
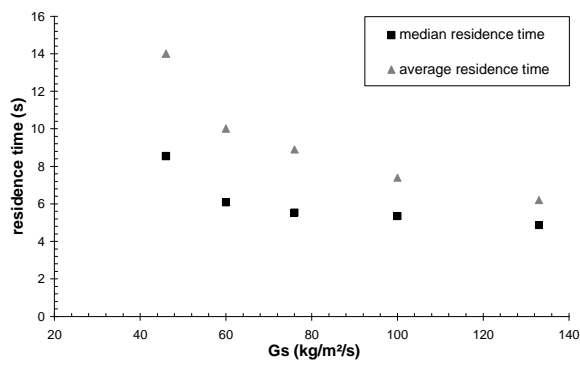*(a) : 46 ; (b) : 60 ; (c) : 76 ; (d) : 100 ; (e) : 133*

(a)

(b)

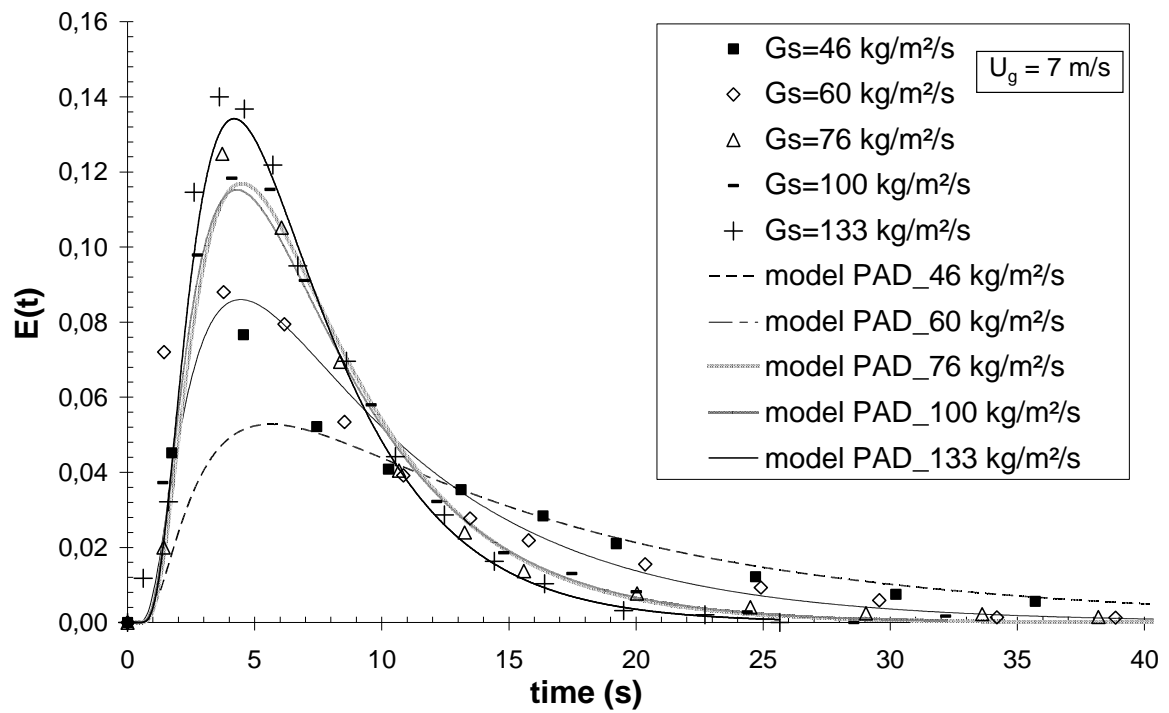*Figure 12. Residence time (a) and spread coefficient (b) evolutions with the solid flux*

Figure 13. RTD modelling with Plug flow model with Axial Dispersion (PAD) for various solid
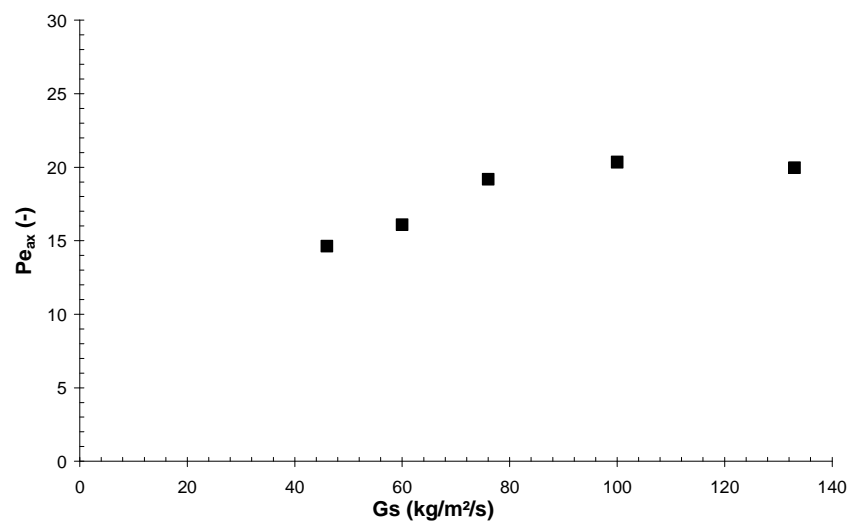
mass fluxes

Figure 14. Peclet number evolution with the solid mass flux